ACS APPLIED MATERIALS & INTERFACES

Research Article

Cite This: ACS Appl. Mater. Interfaces 2019, 11, 11970−11975

www.acsami.org

Measurements of the Thermal Resistivity of InAlAs, InGaAs, and InAlAs/InGaAs Superlattices

G. R. Jaffe,*[,†] S. Mei,[‡] C. Boyle,[‡] J. D. Kirch,[‡] D. E. Savage,[§] D. Botez,[‡] L. J. Mawst,[‡] I. Knezevic,[‡] M. G. Lagally,[§] and M. A. Eriksson[†]

[†]Department of Physics, [‡]Electrical and Computer Engineering, and [§]Materials Science and Engineering, University of Wisconsin−Madison, Madison, Wisconsin 53706, United States

Supporting Information

ABSTRACT: Thermal management efforts in nanoscale devices must consider both the thermal properties of the constituent materials and the interfaces connecting them. It is currently unclear whether alloy/alloy semiconductor superlattices such as InAlAs/InGaAs have lower thermal conductivities than their constituent alloys. We report measurements of the crossplane thermal resistivity of InAlAs/InGaAs superlattices at room temperature, showing that the superlattice resistivities are larger by a factor of 1.2−1.6 than that of the constituent bulk materials, depending on the strain state and composition. We show that the additional resistance present in these superlattices can be tuned by a factor of 2.5 by altering the lattice mismatch and thereby the phonon-mode mismatch at the interfaces, a principle that is commonly assumed for superlattices but has not been experimentally verified without adding new elements to the layers. We find that the additional resistance in superlattices does not increase significantly when the layer thickness is decreased from 4 to 2 nm. We also report measurements of 250−1000 nm thick films of undoped InGaAs and InAlAs lattice-matched to InP substrates, for there is no published thermal conductivity value for the latter, and we find it to be 2.24 ± 0.09 at 22 °C, which is ∼2.7 times smaller than the widely used estimates.

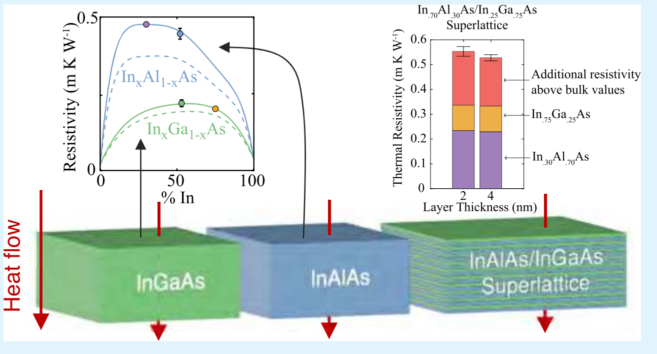

KEYWORDS: *thermal conductivity, thermal resistivity, superlattice, InAlAs, InGaAs, quantum cascade laser*

1. INTRODUCTION

Proper thermal management of nanostructured devices requires understanding phonon transport in both the bulk materials and across the interfaces between them.[1,2] Measurements have shown that epitaxially grown semiconductor superlattices of Si/Ge,[3,4] GaAs/AlAs,[5] and InAs/AlSb[6] with thin layers and high interface densities have up to an order of magnitude lower thermal conductivity, κ, than bulk films of the constituent materials. The materials in those superlattices were either elemental or ordered-binary semiconductors, whose intrinsic thermal conductivity is reasonably high. Conversely, semiconductor random alloys such as $In_xGa_{1-x}As$ have much lower intrinsic thermal conductivities because of the rapid scattering of phonons by alloy atoms,[7,8] and it is an open question whether superlattices of two of these random alloys would see any reduction in thermal conductivity when compared to bulk films of the constituent alloys. Previous work has shown that, at least in certain circumstances, the answer is negative: alloy/alloy superlattices of $Si_{0.84}Ge_{0.16}$/$Si_{0.76}Ge_{0.24}$ showed no measurable reduction in thermal conductivity than the equivalent SiGe alloy.[9] Those alloys, however, had relatively little lattice mismatch between layers, of order 0.4%, and therefore had little phonon-mode mismatch. Further, measurements of the thermal conductivity of SiGe/SiGe superlattices with larger lattice mismatches were found to be dominated by growth defects.[10] Thus, despite the technological importance of alloy/alloy superlattices, it is currently unknown whether ultrathin layers and correspondingly high interface densities produce any measurable decrease in the thermal conductivity of alloy/alloy superlattices.

Ternary alloy semiconductors are technologically very important random alloys. For example, $In_xAl_{1-x}As/In_yGa_{1-y}As$ is widely used in optoelectronic applications such as quantum cascade lasers (QCLs).[11−14] It is crucial for proper thermal management of such devices to understand the fundamental origin of thermal resistance and how it depends on alloy concentration, layer thickness, interface density, and lattice mismatch between layers. In comparison with bulk materials, superlattices are predicted to have larger reductions in their cross-plane thermal conductivities than their in-plane conductivities.[15,16] Furthermore, the majority of the heat in QCL structures is dissipated in the cross-plane direction.[17] The cross-plane thermal conductivity of InAlAs/InGaAs superlattices lattice-matched to InP has been measured,[18] but the

Received: October 3, 2018
Accepted: February 26, 2019
Published: February 26, 2019

thermal conductivity of bulk InAlAs had not been reported at that time, making it difficult to determine whether alloy/alloy superlattices demonstrate any experimentally measurable increase in thermal resistance. Additionally, ternary alloy superlattices are typically grown such that each layer has a different lattice constant than the previous one, with alternating compressively and tensilely strained layers, leading to what are known as strain-balanced (or strain-compensated) heterostructures.[19] This approach allows for a high degree of control over the electrical properties of the superlattice; however, the effect of this lattice mismatch on the thermal conductivity of the superlattice has never been quantified.

Here, we report cross-plane thermal conductivity measurements of InAlAs/InGaAs superlattices, demonstrating that the ultrathin layers and correspondingly high density of interfaces together cause the superlattices to be 1.2−1.6 times as resistive as equivalent amounts of their bulk constituents. These superlattices are composed of the most resistive InAlAs and InGaAs alloys, suggesting that superlattices with other alloy concentrations could see even larger fractional increases in their resistivity. We quantify the effect of phonon-mode mismatch between superlattice layers by comparing lattice-matched superlattices, whose layers have identical lattice constants, and strain-balanced superlattices, which have ∼3% lattice mismatch between each layer and therefore a larger phonon-mode mismatch. We find that the strain-balanced superlattices are ∼60% more resistive than the equivalent amount of bulk material, approximately three times larger than the ∼20% increase measured in lattice-matched superlattices. We find that the resistivity of these superlattices does not depend strongly on layer thickness in the technologically relevant range of 2−4 nm. We compare the superlattice resistivities to measurements of thermal resistivity of thick films of $In_{0.52}Al_{0.48}As$ and $In_{0.53}Ga_{0.47}As$ lattice-matched to their InP substrates at 22 °C. The former has not been measured previously, and we find it to be 2.24 ± 0.09 W m^{-1} K^{-1}. The latter we measure to be 4.57 ± 0.24 W m^{-1} K^{-1}, in agreement with previous results.[20−22]

2. RESULTS

To understand how thermal transport is modified in superlattices, the thermal conductivity of the constituent materials must first be measured. Although both InGaAs and InAlAs are important and widely used, surprisingly the thermal conductivity of undoped InAlAs has not been reported. Further, theoretical results from other ternary alloys are difficult to apply to InAlAs because the light mass of Al has a large impact on the mass scattering terms needed in such calculations.[16,23] To measure the bulk thermal conductivity, thick epitaxial films are required, and these can be grown for both InGaAs and InAlAs when they are lattice-matched to InP, corresponding to $In_{0.53}Ga_{0.47}As$ and $In_{0.52}Al_{0.48}As$. We grow such films with several different thicknesses and then fabricate an array of metal heaters across the surface of each film. We measure the cross-plane thermal resistance of each film using the differential 3ω technique.[24,25] A diagram of a typical sample can be seen in Figure 1. The heaters are 25 μm wide to ensure that the heat flow through the grown films (which are all less than 1 μm thick) is one-dimensional in the cross-plane direction. To improve the precision and understand the uncertainty of the measurements, we average results from many different heaters, typically between 10 and 20, on each sample. For a film thick enough to behave similarly to a bulk material, the thermal resistivity $\rho = 1/\kappa$ (units of m K W^{-1}), is given by $\rho = \frac{R_T \cdot A}{d}$, where R_T is the cross-plane thermal resistance, A is the area of the heater, and d is the film thickness. Figure 2 shows $R_T \cdot A$ of the InAlAs (blue) and InGaAs (green) films as a function of film thickness. The trend of $R_T \cdot A$ is linear with thickness, as expected. We find the thermal conductivity of $In_{0.52}Al_{0.48}As$ to be 2.24 ± 0.09 W m^{-1} K^{-1}. The value we measure is slightly lower than the value of 2.9 ± 0.3 W m^{-1} K^{-1} reported by Koh et al.[26] for $In_{0.52}Al_{0.48}As$ with 0.3% ErAs doping. Importantly, the thermal conductivity we measure is a factor of ∼2.7 lower than the commonly assumed value, which is on the order of 6 W m^{-1} K^{-1}.[27−30] For completeness, we also measure the thermal conductivity of $In_{0.53}Ga_{0.47}As$ and find it to be 4.57 ± 0.24 W m^{-1} K^{-1}, in reasonable agreement with the commonly used value of 5 W m^{-1} K^{-1}.[20] We also measure the temperature dependence of the thermal conductivity of the ∼1 μm thick $In_{0.52}Al_{0.48}As$ and $In_{0.53}Ga_{0.47}As$ samples, and these results can be found in Figure S6 of the Supporting Information. We also provide in Figure S5 the measurements of the temperature-dependent thermal conductivity of the InP substrates under these films, which are in good agreement with the existing literature values.

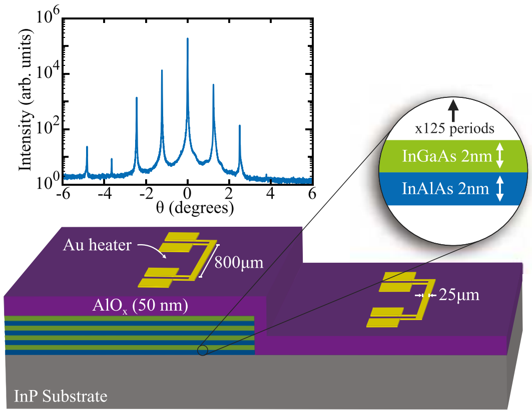

Figure 1. Schematic cross section of a superlattice sample with an AlO_x dielectric capping layer and 3ω heaters. The relative dimensions are exaggerated for clarity. The inset X-ray diffraction data show the 2 nm superlattice periodicity for a strain-balanced superlattice sample. The 3ω heaters are all 25 μm wide with an inner probe spacing of 800 μm and outer probe spacing of 1 mm.

The layers in the strain-balanced superlattices of $In_{0.30}Al_{0.70}As$ and $In_{0.75}Ga_{0.25}As$ each have a ∼1.5% difference in lattice constant compared to InP, with an opposite sign. The resulting strain makes it difficult to grow dislocation-free thick films of the individual alloys on InP for thermal measurements. To estimate the thermal conductivity of the alloys at the corresponding bulk compositions and thus of each of the layers in the superlattice, we use a calculation based on the virtual crystal approximation (VCA).[7] A recent paper by some of us suggests that one important parameter in this calculation, the mass-difference scattering rate, is underestimated in the VCA for III−V ternary alloys.[16] Because of this effect, we adjust this parameter so that the calculated thermal resistivities agree with the values reported above for InAlAs and InGaAs lattice-matched to InP. This adjustment is made by scaling the mass-difference scattering rate reported in ref 16 by 1.39 and 1.32 for InGaAs and InAlAs, respectively. Using the VCA with the scaled mass-difference scattering rate, the estimated thermal conductivity of $In_{0.30}Al_{0.70}As$ is 2.10 W m^{-1} K^{-1} and of

DOI: 10.1021/acsami.8b17268
ACS Appl. Mater. Interfaces 2019, 11, 11970−11975

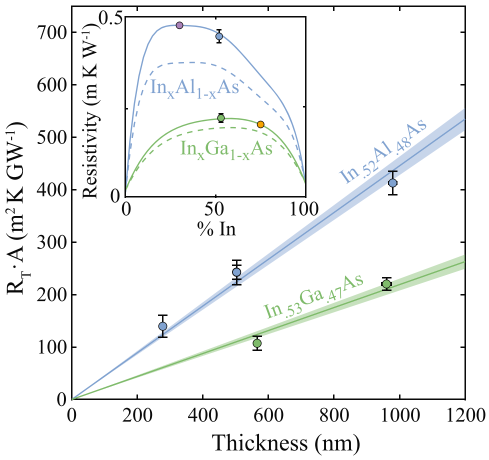

Figure 2. Measured cross-plane thermal resistance R_T times the device area A as a function of film thickness of InAlAs and InGaAs lattice-matched to InP substrates. In the bulk regime, $R_T{\cdot}A$ is linear with film thickness, as seen here. The slope of the fitted lines yields a measurement of the thermal resistivity $\rho = 1/\kappa$, shown as the blue and green points in the inset. For $In_{0.52}Al_{0.48}As$, $\rho = 0.446 \pm 0.018$ m K W^{-1}, and for $In_{0.53}Ga_{0.47}As$, $\rho = 0.219 \pm 0.011$ m K W^{-1}. The shaded regions around the fitted lines in the large plot are the one standard deviation confidence interval of the linear fit. Each point represents an average of 4 to 12 device pairs on a single sample. Vertical error bars represent the uncertainty in the thermal resistance measurement including the device to device variation on a single sample. Measurements of two different growths of 500 nm-thick InAlAs yielded nearly identical resistances. Thickness error bars are also plotted for all points; however, for most points, the error bars are smaller than the plotted point size. The inset shows the measured thermal resistivity of InAlAs (blue point) and InGaAs (green point) as a function of alloy concentration. The inset also includes a calculation of the thermal resistivity of both alloys using the VCA. The mass-difference scattering rate of the original calculation in ref 16 (dashed lines) was scaled (solid lines) to match the measured resistivities, thereby providing an estimate for the resistivity of the alloys in the strain-balanced superlattices (orange and purple points), which could not be measured.

$In_{0.75}Ga_{0.25}As$ is 4.97 W m^{-1} K^{-1}, as shown by purple and orange dots, respectively, in the inset of Figure 2. It is worth noting that although the VCA can accurately predict the thermal resistivity as a function of alloy concentration, simulations have shown that the phonon information extracted from this model, such as relaxation times, is often misrepresented for high-frequency phonons when the mass difference between alloy atoms is large.[31] Fortunately, the analysis here only requires a prediction of the thermal resistivity, which is unaffected by this limitation.

To quantify the effect of layer thickness and phonon-mode mismatch in InAlAs/InGaAs superlattices, we grow two classes of samples: lattice-matched superlattices of $In_{0.52}Al_{0.48}As$/$In_{0.53}Ga_{0.47}As$ and strain-balanced superlattices of $In_{0.30}Al_{0.70}As$/$In_{0.75}Ga_{0.25}As$. For each class, two sets of superlattices are grown, with either 2 or 4 nm thick layers. Two lattice-matched superlattices with 4 nm thick layers are grown, one with 62 and the other 125 repetitions (total thickness of ∼500 nm and ∼1 μm, respectively), to confirm that the thermal resistance of the superlattices is linear with film thickness. The remaining superlattice films are grown with sufficient repetitions to be ∼500 nm thick. Structurally, these two types of heterostructures appear to be equally good, as seen in atomic force microscopy (AFM) surface-roughness measurements and X-ray diffraction profiles. Cross-sectional transmission electron microscopy images of similar superlattices grown by us show that the grown films are single crystal, and we measure X-ray reciprocal space maps of the samples in this work to confirm that there is no relaxation in the strained-balanced superlattices (see the Supporting Information). We average the measurements of multiple heater devices on each sample to extract meaningful error bars (see Experimental Methods below). Figure 3 reports the thermal resistivities of both lattice-matched and strain-balanced superlattices as a function of layer thickness. The resistivity of the equivalent amount of bulk alloy is shown using green, blue, purple, and orange colored bars, and the additional superlattice resistivity above these values is shaded in red. On average, the lattice-matched superlattice resistivity is larger by a factor of 1.2, and the strain-balanced superlattice by a factor of 1.6 than the average resistivity of their constituent alloys. In Figure S6 of the Supporting Information, we show that there is very little temperature dependence to the thermal conductivity of the lattice-matched superlattice with 125 repetitions of $In_{0.52}Al_{0.48}As$ (2 nm)/$In_{0.53}Ga_{0.47}As$ (2 nm).

3. DISCUSSION

Our results demonstrate that alloy/alloy semiconductor superlattices can be more thermally resistive than equivalent amounts of their constituent alloys, despite the relatively high thermal resistivity of random alloy materials. Phonon-mode mismatch between layers, which scales with the lattice mismatch at the interface,[32,33] is also important, and we find that superlattices with a 3% lattice mismatch between layers have 2.5 times the additional thermal resistance than lattice-matched superlattices of identical layer thicknesses. This result suggests that the resistivity of InAlAs/InGaAs superlattices could be increased even further with larger lattice mismatches. Our findings are consistent with the trends reported in the literature for the thermal performance of buried-heterostructure (BH) QCLs. Devices with core regions made of ∼3% lattice-mismatch superlattices have been found to have thermal resistance values ∼40% larger than BH QCLs with core-regions made of ∼2% lattice-mismatch superlattices.[14]

An important result shown in Figure 3 is that the excess thermal resistivities of III−V ternary superlattices above the value expected from bulk resistivities depends only weakly on the layer thicknesses and density of interfaces. Thus, a series resistor model attributing a simple additive resistance to each interface does not fit the data. If a series resistor model were valid, the thermal resistivity would scale inversely with the layer thickness. For the strain-balanced superlattice, the measured additional resistivity is large enough to make it clear that such a scaling does not match the measurement. This comparison is shown graphically in Figure 3c, where we run a one-over-thickness curve through the 4 nm data point and show the divergence that a series resistance model predicts cannot fit the data.

This flattening of the resistivity as the layer thickness decreases is physically reasonable and has been previously observed by Ravichandran et al. in oxide superlattices.[34] In that work, this phenomenon was described as a cross-over regime between coherent and incoherent phonon transport. In coherent phonon transport, the average phonon mean free path is comparable to the layer thickness and interface spacing, which requires that wave-interference effects be considered.[35,36] Experimental evidence for coherent phonon trans-

DOI: 10.1021/acsami.8b17268
ACS Appl. Mater. Interfaces 2019, 11, 11970−11975

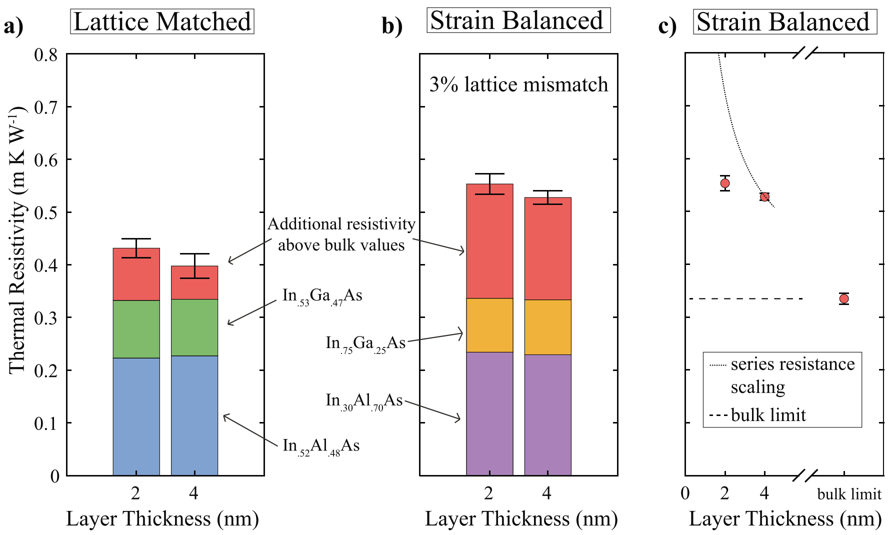

Figure 3. Total bar height is the measured resistivity of (a) lattice-matched and (b) strain-balanced superlattices with colored bars indicating what the resistivity of an equivalent amount of the constituent alloys with no interfaces would be. All of the superlattices are more resistive than equivalent amounts of their bulk constituents, and the red bars indicate that increase in resistivity. The resistivity of the alloys in the lattice-matched superlattices were directly measured (see Figure 2), and the resistivities of the alloy compositions in the strain-balanced superlattices are extracted from the VCA calculation shown in the inset of Figure 2. The error bars in (a,b) include the uncertainty of both the superlattice resistivity measurements and the measured resistivity of bulk alloy films shown in Figure 2. Panel (c) plots the resistivity of the strain-balanced superlattices as a function of layer thickness, and the bulk limit corresponds to the average resistivity of the constituent alloys. The dotted line is chosen to run through the 4 nm data point and scale inversely with layer thickness, as described in the main text.

port in superlattices also has been found for AlAs/GaAs superlattices.[37] In the cross-over regime between coherent and incoherent transport, the thermal resistivity reaches a maximum as a function of interface density, and thus such a cross-over regime may play a role in the flattening of the resistivity as a function of layer thickness we report in Figure 3c.

Another contributing effect is the diffuse phonon scattering at each interface, which drives the phonon-mode population within each material layer out of equilibrium: when phonons scatter across an interface, they drive the phonon-mode occupation in the region immediately surrounding the interface away from the equilibrium.[15,16] If these out-of-equilibrium states have lower group velocities or shorter relaxation times, the effective thermal conductivity of the material near the interface will be reduced below the typical bulk value. The equilibrium occupation is recovered through successive scattering events as the phonons propagate away from the interface. In the case of a superlattice, if the layer thickness is smaller than the phonon mean free path, then the interface contribution to the cross-plane thermal resistance will not be additive.

$In_{0.52}Al_{0.48}As/In_{0.53}Ga_{0.47}As$ superlattices similar to those we study here were measured in ref 18, where the authors also observed little change in superlattice resistivity as a function of layer thickness. With no published thermal conductivity measurement of InAlAs available at that time, the authors analyzed their data under the simplest reasonable assumption that the thermal conductivity of InAlAs was very small, with an estimated value of 1.2 W m^{-1} K^{-1}, and therefore concluded that there was no thermal resistance introduced by the thinness of the layers or from thermal boundary scattering at the interfaces. Thus, a new contribution here is the measurement of the bulk conductivity of $In_{0.52}Al_{0.48}As$ to be 2.24 ± 0.09 W m^{-1} K^{-1}, a significantly larger value, which indicates that in both studies, the superlattices are more resistive than the constituent bulk materials.

It is reasonable to assume that there is some small amount of atomic interdiffusion near the interfaces because no growth is perfectly abrupt. Our X-ray characterization of these samples and cross-sectional transmission electron microscopy on similar superlattices grown in the same metal−organic chemical vapor deposition (MOCVD) system suggest that the interdiffusion is constrained to within a few monolayers of each interface. Past theoretical work has predicted that interdiffusion between layers could either increase the thermal boundary resistance through diffuse phonon scattering[16] or, in some specific cases, reduce the thermal boundary resistance by increasing the phonon transmission.[38]

It is possible that the thermal resistivity of InGaAs reported here is somewhat larger than the resistivity of an infinitely thick film. Measurements by another group indicate that phonons with mean free paths longer than the film thicknesses studied here (500−1000 nm) could reduce the thermal resistivity of thicker films.[22] The fact that the thermal resistivity we measure for InGaAs is in good agreement with the previous results on InGaAs suggests that this difference is small. Because of the sign of this effect, any such difference would cause superlattices to have an even larger fractional increase in resistivity compared to the average of their bulk constituents than that reported here.

4. CONCLUSIONS

We have demonstrated that lattice-matched superlattices of the most thermally resistive InAlAs/InGaAs alloys are 24% more resistive than a film of equivalent thickness of the constituent alloys with no interfaces. This increase in resistance is found to be 61% for strain-balanced superlattices with ∼3% lattice mismatch between layers, an effect that is 2.5 times larger than for lattice-matched superlattices, demonstrating the importance of phonon-mode mismatch at the interfaces. We also

DOI: 10.1021/acsami.8b17268
ACS Appl. Mater. Interfaces 2019, 11, 11970−11975

provide a measurement of the thermal conductivity of undoped $In_{0.52}Al_{0.48}As$ and a calculation of the thermal conductivity of $In_xAl_{1-x}As$ as a function of alloy concentration using the VCA.

This work offers some insights for thermal management of ternary alloy superlattices. For superlattices with few-nanometer-thick layers, the layer thickness does not appear to be a significant variable in determining the total superlattice cross-plane thermal resistivity. Instead, the lattice mismatch at the interface and the resistivity of the bulk alloys are the primary factors. Device designers aiming to reduce the thermal resistivity of superlattices with layers spaced by only a few nanometers must clearly consider the tradeoff between choosing alloys with lower bulk resistivity, as x approaches 0 or 1 (as seen in the inset of Figure 2), versus increasing the superlattice resistivity through phonon-mode mismatch at the interfaces, which will scale with the lattice mismatch between each superlattice layer.

These results are of particular relevance to QCL design, where thermal management is key to achieving high device performance in continuous-wave (CW) operation.[14] QCL long-term reliable operation is well-known to be a strong function of device self-heating in CW operation, as QCL-device degradation has been shown[39,40] to be primarily the result of a thermal runaway. Minimizing the device self-heating is key to QCL reliable operation at watt-range CW powers, as required for a multitude of applications.[14]

5. EXPERIMENTAL METHODS

The InAlAs/InGaAs samples are grown in a close-coupled showerhead MOCVD system on (100) InP substrates. The growth temperature is fixed at 600 °C, as determined by an in situ pyrometer, and the growth rate is ∼1 Å/s. Trimethylgallium (TMGa), trimethylindium (TMIn), and arsine (AsH_3) are used as the growth gas sources. Each superlattice consists of multiple repetitions of a bilayer period that contains one layer of InAlAs and one of InGaAs. A cross-sectional transmission electron microscopy image, which represents the typical quality of the superlattices studied here, is shown in Figure S1 of the Supporting Information.

We measure the cross-plane thermal resistance with a differential 3ω method.[24,25] We measure many devices on each sample to obtain good statistics. For each 3ω measurement, the uncertainty in the measured resistance fluctuations and temperature calibrations of the heaters is propagated along with the variation in thermal resistance measured from device to device. Between 4 and 12 substrate−film device pairs are tested on each sample; in total, over 150 device pairs are measured. Figure 1 depicts a cross section of a typical sample. All experiments are performed at 22 °C in a temperature-controlled chamber. Representative 3ω scans are shown in Figure S4 of the Supporting Information. The thickness of the grown material is determined with AFM and confirmed with X-ray diffraction. An X-ray reciprocal space map and X-ray reflectivity measurements of two of the superlattice films studied here are provided in the Supporting Information, in Figures S2 and S3, respectively.

We measure 10−20 heaters in total on each sample, and the heaters are measured simultaneously in groups of three or four. In total, this produces 3−6 independent differential measurements of thermal resistance on each sample, with associated uncertainties. For each sample, we average these simultaneous measurements, weighting with the uncertainty in each measurement following the formula in ref 41 for data with nonuniform uncertainties and for the error of a weighted mean. The best-fit resistivities of InAlAs and InGaAs shown in Figure 2 include the uncertainties in both the measured resistance and the film thickness. For this fit, we perform a Monte Carlo simulation of the data, the procedure for which can be found in ref 41 Chapter 5. In Figure 3, the uncertainty in thermal resistivity was calculated by propagating the associated errors in each measured quantity: thermal resistance (as described above) and thickness (measured by AFM).

We consider possible systematic errors from both variations in the thickness of the AlO_x passivation layer and from differences between the thermal interface resistance of AlO_x/InAlAs, AlO_x/InGaAs, and AlO_x/InP and estimate both to be small compared to the thermal resistances measured here. The typical variation in the thickness of the AlO_x layer across each sample's surface (8 × 8 mm) is <0.5 nm. Using the typical thermal conductivity of AlO_x of ∼20 W m^{-1} K^{-1}, we estimate that the variation in thermal resistance because of the AlO_x is <0.25 m^2 K GW^{-1} across a sample's surface, which is much smaller than the 250−1000 m^2 K GW^{-1} resistance of the films in this work. The AlO_x/InGaAs thermal interface resistance has been measured to be 10−14 m^2 K GW^{-1},[18] and it is reasonable to assume that the AlO_x/InP interface resistance is close to this value, and therefore the difference between these resistances is expected to be negligible compared to the total film resistances of 250−1000 m^2 K GW^{-1}.

■ ASSOCIATED CONTENT

Supporting Information

The Supporting Information is available free of charge on the ACS Publications website at DOI: 10.1021/acsami.8b17268.

Temperature-dependent thermal conductivity measurements, cross-sectional transmission electron microscopy image, X-ray scattering data, and representative 3ω scans (PDF)

■ AUTHOR INFORMATION

Corresponding Author

*E-mail: gjaffe@wisc.edu.

ORCID

G. R. Jaffe: 0000-0003-2672-0375

Notes

The authors declare no competing financial interest.

■ ACKNOWLEDGMENTS

This work is principally supported by the United States Department of Energy (DOE), Basic Energy Sciences, award #DE-FG02-03ER46028. Growth of III−V materials is supported under Navy contracts N68335-11-C-0432 and N68335-15-C-0073, and Army contract W911NF-16-C-0116. The work of I.K. is supported by DOE award #DE-SC0008712, NSF grant #1702561, and AFOSR grant #FA9550-18-1-0340. We acknowledge the use of facilities supported by NSF through the UW-Madison MRSEC (DMR-1720415).

■ REFERENCES

(1) Cahill, D. G.; Ford, W. K.; Goodson, K. E.; Mahan, G. D.; Majumdar, A.; Maris, H. J.; Merlin, R.; Phillpot, S. R. Nanoscale Thermal Transport. *J. Appl. Phys.* **2003**, *93*, 793−818.

(2) Pop, E. Energy Dissipation and Transport in Nanoscale Devices. *Nano Res.* **2010**, *3*, 147−169.

(3) Lee, S.-M.; Cahill, D. G.; Venkatasubramanian, R. Thermal Conductivity of Si-Ge Superlattices. *Appl. Phys. Lett.* **1997**, *70*, 2957−2959.

(4) Borca-Tasciuc, T.; Liu, W.; Liu, J.; Zeng, T.; Song, D. W.; Moore, C. D.; Chen, G.; Wang, K. L.; Goorsky, M. S.; Radetic, T.; Gronsky, R.; Koga, T.; Dresselhaus, M. S. Thermal Conductivity of Symmetrically Strained Si/Ge Superlattices. *Superlattices Microstruct.* **2000**, *28*, 199−206.

(5) Capinski, W. S.; Maris, H. J.; Ruf, T.; Cardona, M.; Ploog, K.; Katzer, D. S. Thermal-Conductivity Measurements of GaAs/AlAs Superlattices Using a Picosecond Optical Pump-and-Probe Technique. *Phys. Rev. B: Condens. Matter Mater. Phys.* **1999**, *59*, 8105−8113.

(6) Borca-Tasciuc, T.; Achimov, D.; Liu, W.; Chen, G.; Ren, H.; Lin, C.; Pei, S. Thermal Conductivity of InAs/AlSb Superlattices. *Microscale Thermophys. Eng.* **2001**, *5*, 225−231.

(7) Abeles, B. Lattice Thermal Conductivity of Disordered Semiconductor Alloys at High Temperatures. *Phys. Rev.* **1963**, *131*, 1906−1911.

(8) Adachi, S. Lattice Thermal Conductivity of Group−IV and III−V Semiconductor Alloys. *J. Appl. Phys.* **2007**, *102*, 063502.

(9) Huxtable, S. T.; Abramson, A. R.; Tien, C.-L.; Majumdar, A.; Labounty, C.; Fan, X.; Zeng, G.; Bowers, J. E.; Shakouri, A.; Croke, E. T. Thermal Conductivity of Si/SiGe and SiGe/SiGe Superlattices. *Appl. Phys. Lett.* **2002**, *80*, 1737−1739.

(10) Huxtable, S. T. Heat Transport in Superlattices and Nanowire Arrays. Ph.D. Thesis, University of California, Berkeley, CA, USA, 2002, 100−104.

(11) Faist, J.; Capasso, F.; Sivco, D. L.; Sirtori, C.; Hutchinson, A. L.; Cho, A. Y. Quantum Cascade Laser. *Science* **1994**, *264*, 553−556.

(12) Köhler, R.; Tredicucci, A.; Beltram, F.; Beere, H. E.; Linfield, E. H.; Davies, A. G.; Ritchie, D. A.; Iotti, R. C.; Rossi, F. Terahertz Semiconductor-Heterostructure Laser. *Nature* **2002**, *417*, 156−159.

(13) Xie, F.; Caneau, C. G.; LeBlanc, H. P.; Visovsky, N. J.; Coleman, S.; Hughes, L. C.; Zah, C.-e. High-temperature continuous-wave operation of low power consumption single-mode distributed-feedback quantum-cascade lasers at $\lambda \sim 5.2$ μm. *Appl. Phys. Lett.* **2009**, *95*, 091110.

(14) Botez, D.; Chang, C.-C.; Mawst, L. J. Temperature sensitivity of the electro-optical characteristics for mid-infrared (λ = 3-16μm)-emitting quantum cascade lasers. *J. Phys. D: Appl. Phys.* **2016**, *49*, 043001.

(15) Aksamija, Z.; Knezevic, I. Thermal Conductivity of $Si_{1-x}Ge_x$/$Si_{1-y}Ge_y$ Superlattices: Competition Between Interfacial and Internal Scattering. *Phys. Rev. B: Condens. Matter Mater. Phys.* **2013**, *88*, 155318.

(16) Mei, S.; Knezevic, I. Thermal Conductivity of III-V Semiconductor Superlattices. *J. Appl. Phys.* **2015**, *118*, 175101.

(17) Lops, A.; Spagnolo, V.; Scamarcio, G. Thermal modeling of GaInAs/AlInAs quantum cascade lasers. *J. Appl. Phys.* **2006**, *100*, 043109.

(18) Sood, A.; Rowlette, J. A.; Caneau, C. G.; Bozorg-Grayeli, E.; Asheghi, M.; Goodson, K. E. Thermal conduction in lattice-matched superlattices of InGaAs/InAlAs. *Appl. Phys. Lett.* **2014**, *105*, 051909.

(19) Faist, J.; Capasso, F.; Sivco, D. L.; Hutchinson, A. L.; Chu, S.-N. G.; Cho, A. Y. Short wavelength ($\lambda \sim 3.4$ μm) quantum cascade laser based on strained compensated InGaAs/AlInAs. *Appl. Phys. Lett.* **1998**, *72*, 680−682.

(20) Abrahams, M. S.; Braunstein, R.; Rosi, F. D. Thermal, Electrical and Optical Properties of (In,Ga)as Alloys. *J. Phys. Chem. Solids* **1959**, *10*, 204−210.

(21) Kim, W.; Zide, J.; Gossard, A.; Klenov, D.; Stemmer, S.; Shakouri, A.; Majumdar, A. Thermal Conductivity Reduction and Thermoelectric Figure of Merit Increase by Embedding Nanoparticles in Crystalline Semiconductors. *Phys. Rev. Lett.* **2006**, *96*, 045901.

(22) Koh, Y. K.; Cahill, D. G. Frequency Dependence of the Thermal Conductivity of Semiconductor Alloys. *Phys. Rev. B: Condens. Matter Mater. Phys.* **2007**, *76*, 075207.

(23) Adachi, S. Lattice thermal resistivity of III-V compound alloys. *J. Appl. Phys.* **1983**, *54*, 1844−1848.

(24) Cahill, D. G. Thermal conductivity measurement from 30 to 750 K: the 3ω method. *Rev. Sci. Instrum.* **1990**, *61*, 802−808.

(25) Schroeder, D. P.; Aksamija, Z.; Rath, A.; Voyles, P. M.; Lagally, M. G.; Eriksson, M. A. Thermal Resistance of Transferred-Silicon-Nanomembrane Interfaces. *Phys. Rev. Lett.* **2015**, *115*, 256101.

(26) Koh, Y. K.; Singer, S. L.; Kim, W.; Zide, J. M. O.; Lu, H.; Cahill, D. G.; Majumdar, A.; Gossard, A. C. Comparison of the 3ω method and time-domain thermoreflectance for measurements of the cross-plane thermal conductivity of epitaxial semiconductors. *J. Appl. Phys.* **2009**, *105*, 054303.

(27) Spagnolo, V.; Troccoli, M.; Scamarcio, G.; Gmachl, C.; Capasso, F.; Tredicucci, A.; Sergent, A. M.; Hutchinson, A. L.; Sivco, D. L.; Cho, A. Y. Temperature profile of GaInAs/AlInAs/InP quantum cascade-laser facets measured by microprobe photoluminescence. *Appl. Phys. Lett.* **2001**, *78*, 2095−2097.

(28) Kim, Y. M.; Rodwell, M. J. W.; Gossard, A. C. Thermal Characteristics of InP, InAlAs, and AlGaAsSb Metamorphic Buffer Layers Used in $In_{0.52}Al_{0.48}As/In_{0.53}Ga_{0.47}As$ Heterojunction Bipolar Transistors Grown on GaAs Substrates. *J. Electron. Mater.* **2002**, *31*, 196−199.

(29) Yang, H.; Wang, H.; Radhakrishnan, K.; Tan, C. L. Thermal Resistance of Metamorphic InP-Based HBTs on GaAs Substrates Using a Linearly Graded $In_xGa_{1-x}P$ Metamorphic Buffer. *IEEE Trans. Electron Devices* **2004**, *51*, 1221−1227.

(30) Lee, H. K.; Yu, J. S. Thermal Analysis of Short Wavelength InGaAs/InAlAs Quantum Cascade Lasers. *Solid-State Electron.* **2010**, *54*, 769−776.

(31) Larkin, J. M.; McGaughey, A. J. Predicting Alloy Vibrational Mode Properties Using Lattice Dynamics Calculations, Molecular Dynamics Simulations, and the Virtual Crystal Approximation. *J. Appl. Phys.* **2013**, *114*, 023507.

(32) Swartz, E. T.; Pohl, R. O. Thermal Boundary Resistance. *Rev. Mod. Phys.* **1989**, *61*, 605−668.

(33) Chen, G.; Zeng, T. Nonequilibrium Phonon and Electron Transport in Heterostructures and Superlattices. *Microscale Thermophys. Eng.* **2001**, *5*, 71−88.

(34) Ravichandran, J.; Yadav, A. K.; Cheaito, R.; Rossen, P. B.; Soukiassian, A.; Suresha, S. J.; Duda, J. C.; Foley, B. M.; Lee, C.-H.; Zhu, Y.; Lichtenberger, A. W.; Moore, J. E.; Muller, D. A.; Schlom, D. G.; Hopkins, P. E.; Majumdar, A.; Ramesh, R.; Zurbuchen, M. A. Crossover from Incoherent to Coherent Phonon Scattering in Epitaxial Oxide Superlattices. *Nat. Mater.* **2014**, *13*, 168−172.

(35) Simkin, M. V.; Mahan, G. D. Minimum Thermal Conductivity of Superlattices. *Phys. Rev. Lett.* **2000**, *84*, 927−930.

(36) Chen, G. Thermal Conductivity and Ballistic-Phonon Transport in the Cross-Plane Direction of Superlattices. *Phys. Rev. B: Condens. Matter Mater. Phys.* **1998**, *57*, 14958−14973.

(37) Luckyanova, M. N.; Garg, J.; Esfarjani, K.; Jandl, A.; Bulsara, M. T.; Schmidt, A. J.; Minnich, A. J.; Chen, S.; Dresselhaus, M. S.; Ren, Z.; Fitzgerald, E. A.; Chen, G. Coherent Phonon Heat Conduction in Superlattices. *Science* **2012**, *338*, 936−939.

(38) Tian, Z.; Esfarjani, K.; Chen, G. Enhancing Phonon Transmission Across a Si/Ge Interface by Atomic Roughness: First-Principles Study with the Green's Function Method. *Phys. Rev. B: Condens. Matter Mater. Phys.* **2012**, *86*, 235304.

(39) Zhang, Q.; Liu, F.-Q.; Zhang, W.; Lu, Q.; Wang, L.; Li, L.; Wang, Z. Thermal Induced Facet Destructive Feature of Quantum Cascade Lasers. *Appl. Phys. Lett.* **2010**, *96*, 141117.

(40) Sin, Y.; Lingley, Z.; Brodie, M.; Presser, N.; Moss, S. C.; Kirch, J.; Chang, C.-C.; Boyle, C.; Mawst, L. J.; Botez, D.; Lindberg, D.; Earles, T. Destructive Physical Analysis of Degraded Quantum Cascade Lasers. *Proc. SPIE* **2015**, *9382*, 93821P.

(41) Bevington, P. R.; Robinson, D. K. *Data Reduction and Error Analysis for the Physical Sciences*, 3rd ed.; McGraw-Hill: New York, 1969; pp 51−59 and 75−98.

DOI: 10.1021/acsami.8b17268
ACS Appl. Mater. Interfaces 2019, 11, 11970−11975